



Synthesis of barium oxide nanoparticles and its novel application as a catalyst for the photodegradation of malachite green dye

Falak Naz¹ · Khalid Saeed¹

Received: 7 August 2021 / Accepted: 8 March 2022 / Published online: 15 April 2022
© The Author(s) 2022

Abstract

The synthesis of undoped barium oxide (BaO) and neodymium (Nd)-doped BaO nanoparticles (NPs) was carried out through the co-precipitation technique. The synthesis of cubic structure BaO NPs was confirmed through X-ray diffraction (XRD). The crystallite sizes calculated from X-rays diffractometric (XRD) results for undoped BaO and Nd-doped BaO were 10.50 nm and 10.04 nm, respectively. The morphological study and percent composition of synthesized NPs were investigated using a scanning electron microscope and energy-dispersive X-ray analysis. Thermogravimetric analysis confirmed the decomposition of precursor to BaO after annealing at ~ 500 °C. The band gap energy calculated for undoped BaO was 3.7 eV. The substitution of Nd to BaO decreased this value to 3.4 eV. The activation energy calculated for the doped BaO and undoped BaO was 16.5 kJ/mol and 22.5 kJ/mol, respectively. The Nd-doped BaO degraded about 96.4% dye, while the undoped BaO NPs degraded about 86.6% dye within 120 min. The synthesized BaO NPs were used as novel catalysts for the photodegradation of malachite green (MG) dye by varying irradiation time, catalyst dose, pH, temperatures and dye initial concentration. The maximum degradation efficiency was achieved at pH 4, catalyst dose 10 mg, dye initial concentration 50 ppm, and at a temperature of 50 °C. The dye degradation was also studied using the recovered catalysts.

Keywords Malachite green dye · Nanoparticles · Kinetics · Photocatalyst

Introduction

Water cannot be replaced by men for its daily development, commodities, and industrialization, as it is one of the natural and precious resources. The quality of water across the world is directly affected by rapid industrialization and the enormous increase in population growth (Shivaraju et al. 2017). The development of a country is based on its industrial development. As different industries discard life-threatening wastes into the aquatic systems which badly affects the quality of water (Shah et al. 2016). The textile, printing, food processing, papermaking, cosmetics, and pharmaceutical industries discharge their effluents to the water bodies containing excess amounts of pigments and dyes (Alnuaimi et al. 2007; Avasarala et al. 2016). It has been found to possess neurotoxicity, chronic toxicity, and carcinogenicity toward animals and humans. Before they

become dangerous to the natural environments the removal of dyes from industrial effluents is required (Das, and Bhattacharyya 2014). In addition to destroying the beauty of the river dyes also reduce sunlight penetration through water, due to which the process of photosynthesis in aquatic green plants is also affected (Saeed et al. 2015). To eliminate the dyes from waste-water many methods have been reported in the literature such as adsorption on activated charcoal, cation exchange membrane, chemical degradation, adsorption/precipitation process, micellar enhanced filtration, electrochemical degradation, integrated iron (30 photos-assisted biological treatment, biological treatment scheme, integrated chemical biological degradation, and solar-photo-Fenton reagent, but some flaws have been found in each of these treatment methods (Rafatullah et al. 2010). For example, in adsorption simply dyes/pollutants are transferred from one phase to another which is a non-destructive method. In physical methods, secondary pollutants are produced, while sludge production is a major drawback of biological methods (Yaseen and Scholz 2019). Recently, a superior method to remove dyes or other organic substances from water is photodegradation, because in addition to removing toxic

✉ Falak Naz
falakkaan1@gmail.com

¹ Department of Chemistry, Bacha Khan University,
Charsadda 24420, KPK, Pakistan

pollutants, it also degrades them into non-toxic substances. Photodegradation involves the photochemical breakdown of a molecule into simple, lower molecular weight, and non-toxic fragments due to light exposure in the presence of photocatalyst. Photocatalyst is a semiconducting material activated by the absorption of light and can accelerate the rate and degradation efficiency of photodegradation reaction without being consumed (Dobson and Burgess 2007). The use of photocatalysts had been extensively investigated to decrease the damage caused by dye pollution to humans and the environment (Wang et al. 2007).

In the present study, BaO and Nd-doped BaO NPs were used as novel catalysts for the degradation of malachite green dye. The undoped BaO and Nd-doped BaO NPs were prepared by co-precipitation technique and were characterized through SEM, EDX, XRD, FTIR, TGA. The results of MG degradation by the doped BaO nanoparticles were compared with the undoped BaO nanoparticles.

Experimental

Material

Analytical grade nitrate salts of barium [$\text{Ba}(\text{NO}_3)_2$] and neodymium [$\text{Nd}(\text{NO}_3)_3 \cdot 6\text{H}_2\text{O}$] were obtained from Sigma-Aldrich. Malachite green dye and sodium hydroxide of reagent grade were purchased from Merck chemical company. All the chemicals were used as received. Milli-Q ultra-pure water was used for making the dye solutions.

Synthesis of catalyst

The synthesis of doped and undoped photocatalysts was carried out via the co-precipitation method in the present study. The main advantages of the co-precipitation method over other methods are its reasonable cost, high purity of the product, and its easy reproducibility.

Synthesis of BaO nanoparticles

The synthesis of BaO NPs was carried out by the co-precipitation technique. 1 M sodium hydroxide solution was added to 0.5 M barium nitrate [$\text{Ba}(\text{NO}_3)_2$] solution and stirred at room temperature for 2 h. The solution was then kept undisturbed for 8 h to obtain a precipitate. The impurities in the hydroxide precipitate are removed by washing several times with double distillation. After drying the precipitate in an oven at 80 °C, it was finally calcined at 500 °C for 2 h to obtain BaO nanoparticles.

Synthesis of Nd-doped BaO nanoparticles

The synthesis of Nd-doped BaO NPs was carried out through co-precipitation techniques by the mixing of 0.05 M neodymium nitrate [$\text{Nd}(\text{NO}_3)_3 \cdot 6\text{H}_2\text{O}$] and barium nitrate [$\text{Ba}(\text{NO}_3)_2$] solution. Then, 1 M sodium hydroxide solution was added to the solution and stirred at room temperature for 2 h. The solution was allowed to stand for 8 h to obtain a precipitate. Impurities in the obtained hydroxide precipitate were removed by washing with double distillation several times. After drying the precipitate in an oven at 80 °C, it was finally calcined at 500 °C for 2 h to obtain Nd-doped BaO nanoparticles.

Instrumentation

The morphological study of undoped BaO and Nd-doped BaO was done via SEM (JEOL-JSM 5800). The elemental composition of the sample was studied by an energy-dispersive X-ray analyzer (INCA-200 of Oxford Instruments UK). X-ray diffractometer model (JEOL-JDX-5332 Japan) was used for XRD analysis of nanoparticles. FTIR spectrophotometer model (95,120 PerkinElmer) was used to analyze the infrared spectrum of the catalyst. It was confirmed by TGA (TGA-50, Shimadzu) that the precursor was decomposed into nanoparticles after annealing at about 500 °C at a heating rate of 10 °C/min. The concentration of malachite green dye was analyzed using a Shimadzu UV-1800 dual-beam spectrophotometer.

Photocatalysis

In a self-made photocatalytic reactor, the malachite green dye degradation was carried out in the presence of BaO-NPs under UV-light (254 nm, 15 W) in a homemade photocatalytic reactor. To evaluate the photocatalytic activity of the synthesized nanoparticles, 20 mg of nanoparticles was added to a solution of malachite green dye (50 ppm) in 100 ml of double-distilled water under continuous stirring. The adsorption–desorption equilibrium was established by stirring the reaction mixture in the dark for half an hour. A sample (5 ml) was then taken for testing, and the catalyst was separated by centrifugation before taking UV–Visible readings. Next, the reactor was irradiated with ultraviolet light, and samples were collected periodically and analyzed using ultraviolet–visible spectroscopy (Shimadzu, Japan). Using the following formula to calculate the degradation percentage of the dye.

$$\text{Percent degradation} = \frac{C_0 - C}{C_0} \times 100 \quad (1)$$

where C° and C represent the initial concentration and final concentration of the dye at different time intervals, respectively.

Results and discussion

Scanning electron microscopic investigation

The surface morphology of undoped BaO and Nd-doped BaO NPs was studied by scanning electron microscopy. From the SEM image of undoped BaO (Fig. 1a), it can be concluded that the material is composed of uniformly dispersed, porous, agglomerated, and flower-like nanoparticles. The SEM image of the doped BaO (Fig. 1b) shows that the particles appear in the form of aggregation and dispersion and are irregular in shape.

Elemental composition study

The EDX spectrum of BaO NPs is shown in Fig. 2a, possessing a strong band for Ba and O with elemental weight percent of 77.28 and 22.72, respectively, which confirms the synthesis of BaO NPs. The EDX spectrum of Nd-doped BaO NPs possesses a strong band for Ba, O, and Nd with elemental weight percent of 63.28, 23.01, and 13.71, respectively, as shown in Fig. 2b, which confirms the synthesis of Nd-doped BaO NPs.

Crystallite size of the prepared NPs

The XRD analysis of BaO and Nd-doped BaO NPs is shown in Figs. 3a and 3b. The diffraction peaks are observed at values 23.7° , 24.01° , 29.72° , 35.00° , 44.21° for undoped BaO and 23.9° , 24.15° , 29.82° , 35.04° , 44.82° for Nd-doped BaO corresponding to (100), (101), (111), (110) and (103), respectively. The average grain sizes were calculated from

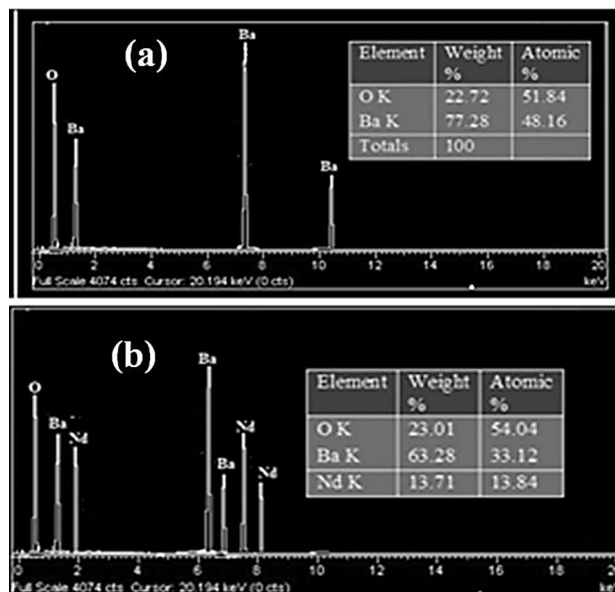


Fig. 2 EDX spectra of **a** undoped BaO and **b** Nd-doped BaO

the peak widths, considering the most intense peak (100) and using the Debye–Scherrer equation.

The average crystallite size of the pure BaO is found to be 10.50 nm which decreases to 10.04 nm in Nd-doped BaO. The nucleation centers density increases with the decrease in grain size leading to the formation of small crystallites. The diffraction peaks were shifted slightly toward higher angles of 2θ in Nd-doped BaO nanopowder as compared to undoped BaO nanopowder. This may be due to a small variation in the particles size (Ramasam et al. 2012).

FTIR spectroscopy

Figure 4a shows the FTIR spectra of undoped BaO NPs. The bands for BaO are presented as a low one at 693 cm^{-1} and intense at 857 cm^{-1} . The absorption band between 1183

Fig. 1 SEM **a** undoped BaO and **b** Nd-doped BaO

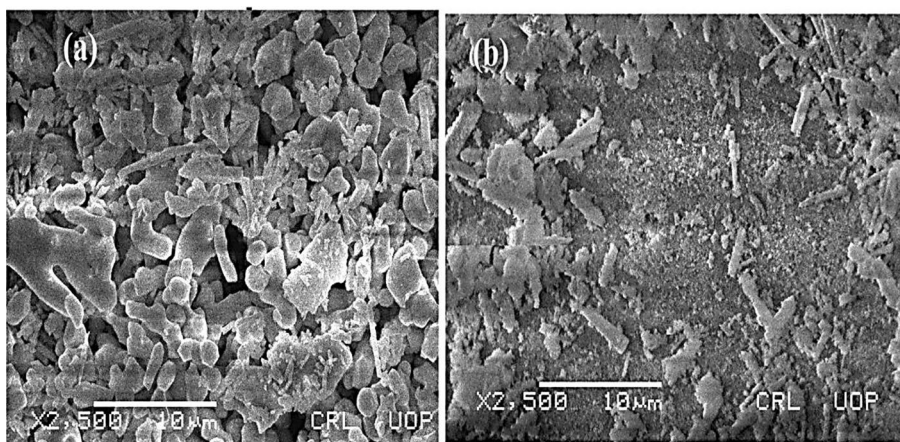


Fig. 3 XRD **a** undoped BaO and **b** Nd-doped BaO

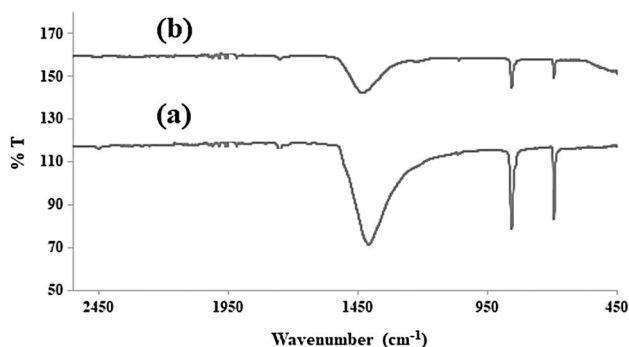
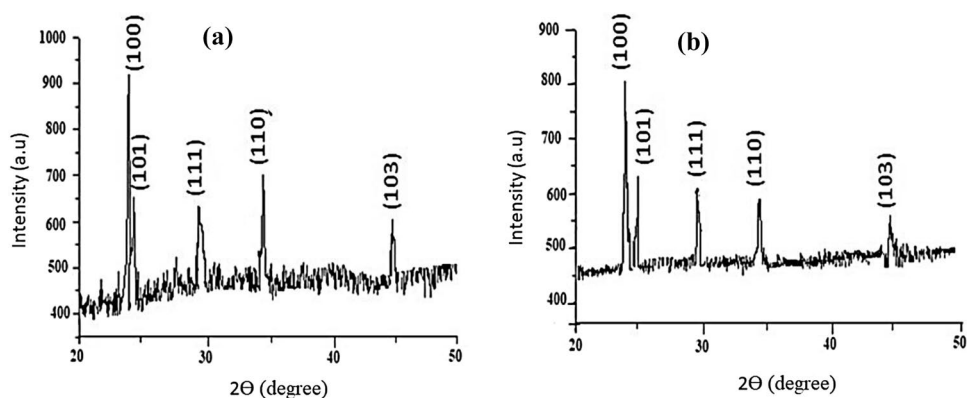
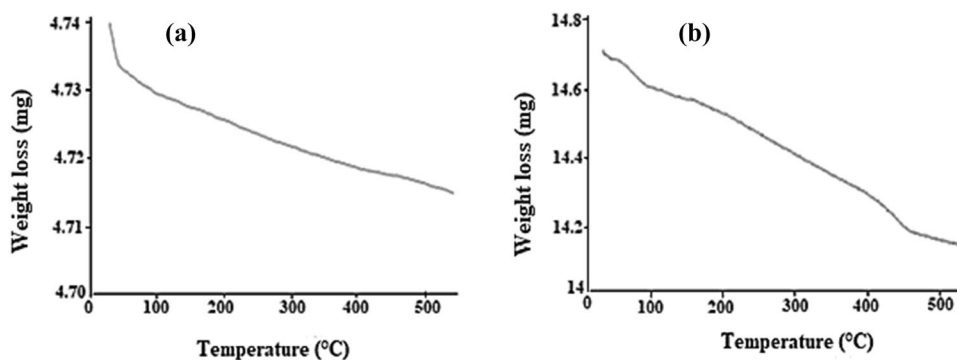


Fig. 4 FTIR spectra of **a** undoped BaO and **b** Nd-doped BaO nanoparticles

and 1582 cm^{-1} is attributed to Ba–O bond stretching. The absence of an absorption band between 3500 and 3000 cm^{-1} indicates that the water molecules are removed completely from the crystal lattice of the catalyst (Wang et al. 2010).

FTIR spectra of Nd-doped BaO NPs are shown in Fig. 4b. The bands for BaO are presented as a low one at 695 cm^{-1} and intense at 858 cm^{-1} . The absorption band between 1293 and 1607 cm^{-1} is attributed to Ba–O–Nd bond stretching. The absence of an absorption band between 3500 and 3000 cm^{-1} indicates that the water molecules are removed completely from the crystal lattice of the catalyst.

Fig. 5 TGA analysis **a** undoped BaO and **b** Nd-doped BaO



Thermal analysis

Thermal analysis (TGA) of BaO and Nd-doped BaO NPs with a heating rate of 10 °C/min . is shown in Fig. 5. A weight loss occurs for both the samples in the range of 50 °C to about 100 °C , which might be due to the dehydration of surface-adsorbed water. A major weightlessness tape occurs in the range of 100 °C to about 400 °C for the undoped BaO and 100 °C to about 450 °C for the doped BaO beyond which there is no weight loss, indicating the loss of OH⁻ (Long et al. 2008).

Optical properties

To record the optical properties of the sample, the UV–Vis absorption spectrophotometer was used. The absorption coefficient (α) is calculated using Eq. 2. Sample thickness (t) and absorbent (A)

$$\alpha = 2.303A/t \quad (2)$$

By extrapolating the linear part of the graph between $(\alpha h\nu)^2$ and photon energy ($h\nu$), until it meets the x-axis the band gap energy is calculated as shown in Fig. 6. The E_g value for BaO nanoparticles is calculated to be 3.7 eV as shown in

Fig. 6a. Doping BaO with Nd has decreased its E_g to 3.4 eV as shown in Fig. 6b.

Photocatalytic kinetics

The first-order kinetics of photodegradation of dyes was estimated at different temperatures using the following equation:

$$\ln C_0/C = k_{app} \cdot t \tag{3}$$

where C_0 denotes the concentration of dye before photodegradation, C denotes the concentration of dye at reaction time t , and k_{app} is the apparent rate constant (min^{-1}). The apparent rate constant (k_{app}) and correlation coefficient (R^2) were calculated from the slope of a plot between $\ln C_0/C$ and time (Fig. 7) and are shown in Table 1. On comparing the rate constant (k) of undoped BaO for the photocatalytic degradation of MG dye with that of Nd-doped BaO, the value of k_{app} in the former case was found to be smaller than that of the latter. The second-order kinetic was also estimated at various temperatures using the following equation:

Fig. 6 Optical band gap **a** undoped BaO and **b** Nd-doped BaO

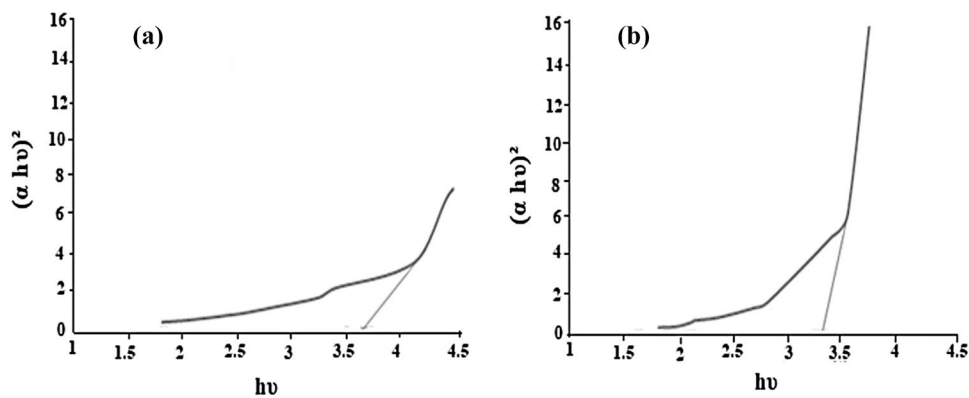


Fig. 7 Application of pseudo-first-order kinetics to photodegradation of dye on **a** undoped and **b** Nd doped BaO at different temperature

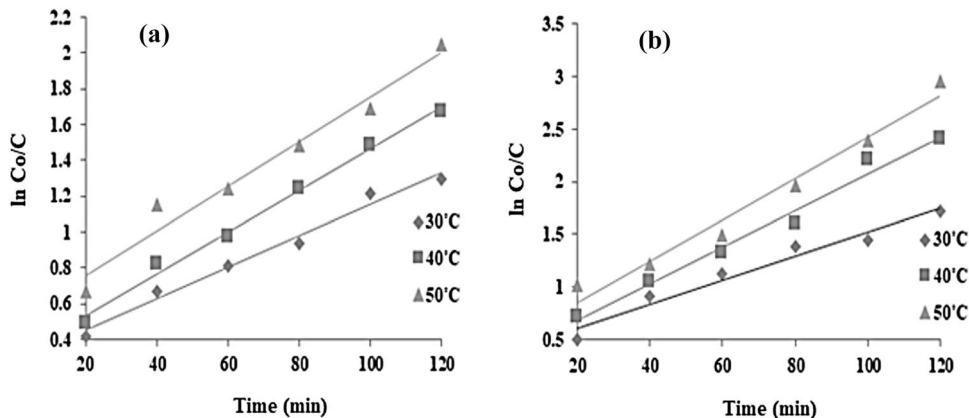


Table 1 Kinetic constant parameter values for the photocatalytic degradation of malachite green dye at different temperatures

Temperature (degree Celsius)	Pseudo-first-order kinetics		Pseudo-second-order kinetics		Activation Energy (KJ/mol)
	K_{app}	R^2	K_{app}	R^2	
Undoped BaO	30	0.008	0.981	0.0004	22.5
	40	0.011	0.992	0.0007	
	50	0.012	0.966	0.0007	
Nd-doped BaO	30	0.011	0.964	0.0007	16.5
	40	0.017	0.982	0.0019	
	50	0.019	0.973	0.0031	

$$1/C - 1/C_0 = k_{app}t \quad (4)$$

where C_0 denotes the concentration of dye before photodegradation, C denotes the concentration of dye at reaction time t , and k_{app} is the apparent rate constant (min^{-1}). The apparent rate constant (k) and correlation coefficient (R^2) were calculated from the slope of a plot between $1/C-1/C_0$ and time (Fig. 8) and are shown in Table 1. On comparing the rate constant (k) of undoped BaO for MG dye degradation with that of Nd-doped BaO, the value of k_{app} in the former case was found to be smaller than that of the latter. However, first-order kinetics best fitted to the experimental data. The values of apparent rate constants measured at temperature 30, 40, and 50 °C over the undoped BaO and Nd-doped BaO catalysts have been used to calculate the activation energy, E_a , values by applying the following equation:

$$\ln k = \ln A - E_a/RT \quad (5)$$

Figure 9 depicts the obtained graph for Nd-doped BaO and BaO where the E_a values calculated from the slope of the graph are 16.5 kJ/mol and 22.5 kJ/mol, respectively, as shown in Table 1.

Fig. 8 Application of pseudo-second-order kinetics to photodegradation of dye on **a** undoped BaO and **b** Nd-doped BaO at different temperatures

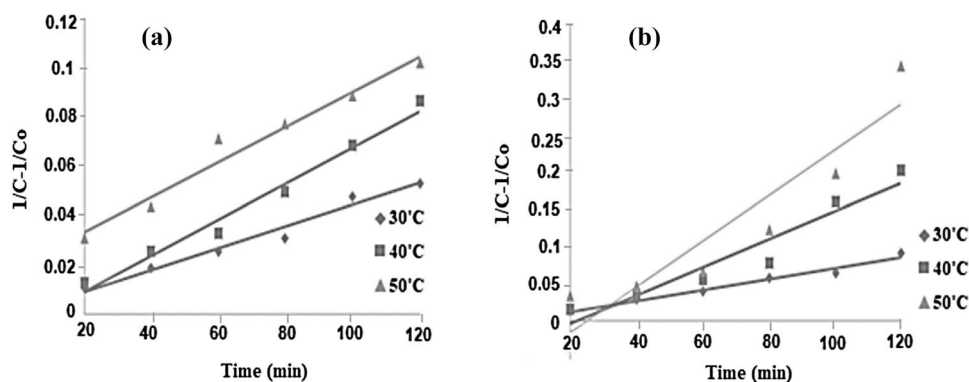
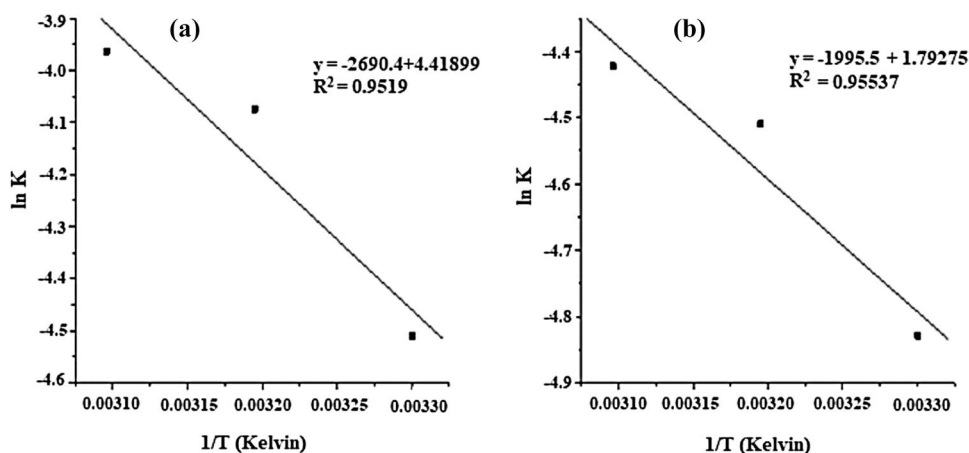


Fig. 9 Application of Arrhenius equation to rate constant (k_{app}) on **a** undoped BaO and **b** Nd-doped BaO



The effect of different concentrations (50–250 mg L^{-1}) of the dye on reaction rate by using 20 mg BaO and Nd-doped BaO as photocatalysts was also studied. The apparent rate constant was calculated by applying the pseudo-first-order kinetic equation to the obtained data. The values of the apparent rate constants and their respective regression coefficients were calculated from the slope of the graph (Fig. 10) at different initial dye concentrations and are shown in Table 2. The apparent rate constants were also calculated by applying the second-order kinetic equation to the obtained data. The apparent rate constant values and their respective regression coefficients were calculated from the slope of the graph (Fig. 11) at different initial dye concentrations, as shown in Table 2. These kinetic parameters indicate that the interaction of BaO and Nd enhances the catalytic performance.

Photodegradation mechanism

The excitation of electron(s) from the valance band (VB) to the conduction band (CB) of the catalyst occurs if UV light of energy greater than the band gap energy of the metal oxide nanoparticles is irradiated over BaO. As a result electrons (e^-) and holes (h^+) are generated in the CB and VB, respectively, as shown in Scheme 1.

Fig. 10 Application of pseudo-first-order kinetics to photodegradation of dye on **a** undoped and **b** Nd-doped BaO at different initial concentrations of dye

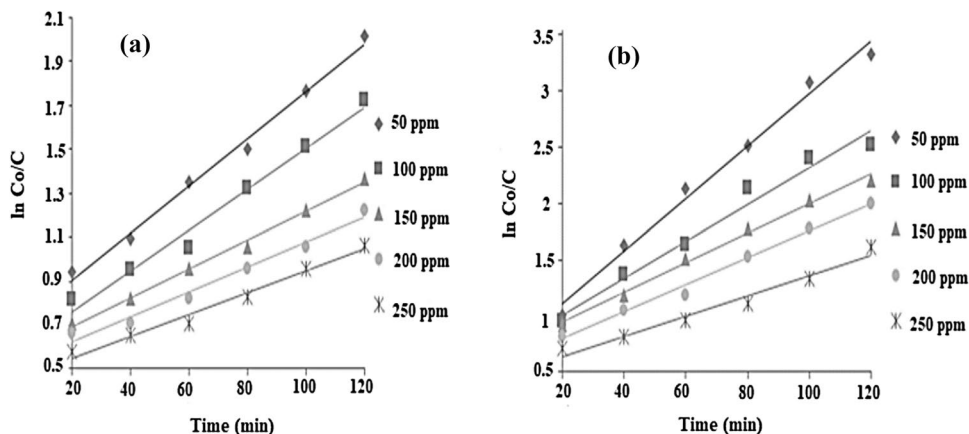


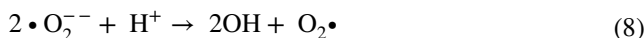
Table 2 Kinetic constant parameter values for the photocatalytic degradation of malachite green dye at different initial concentrations of dye

Concentration (ppm)	Pseudo-first-order kinetics		Pseudo-second-order kinetics		
	K_{app}	R^2	K_{app}	R^2	
Undoped BaO	50	0.010	0.992	0.001	0.9519
	100	0.009	0.982	0.0003	0.949
	150	0.006	0.995	0.0001	0.9761
	200	0.005	0.979	0.00007	0.9571
	250	0.004	0.982	0.00004	0.966
Nd-doped BaO	50	0.023	0.989	0.0051	0.9456
	100	0.016	0.975	0.0011	0.9755
	150	0.013	0.992	0.0004	0.9887
	200	0.012	0.990	0.0003	0.9556
	250	0.008	0.967	0.0001	0.9058

The interaction of the holes and the surface-bound water molecules and OH groups produce reactive hydroxyl radicals.



Photo-excited electrons react with molecular oxygen bound to the surface to produce superoxide ions. The final products of the reduction are usually hydroperoxide radicals and OH radicals.



Hydroxide is a powerful oxidant that will attack organic compounds and cause them to be fully mineralized (Sharma et al. 2020).

Dye degradation by recovered catalyst

The MG dye was also degraded under the same experimental conditions using the recovered photocatalyst, as shown in Fig. 12. The original Nd-doped BaO degraded 96.4% dye

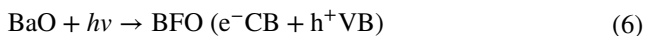
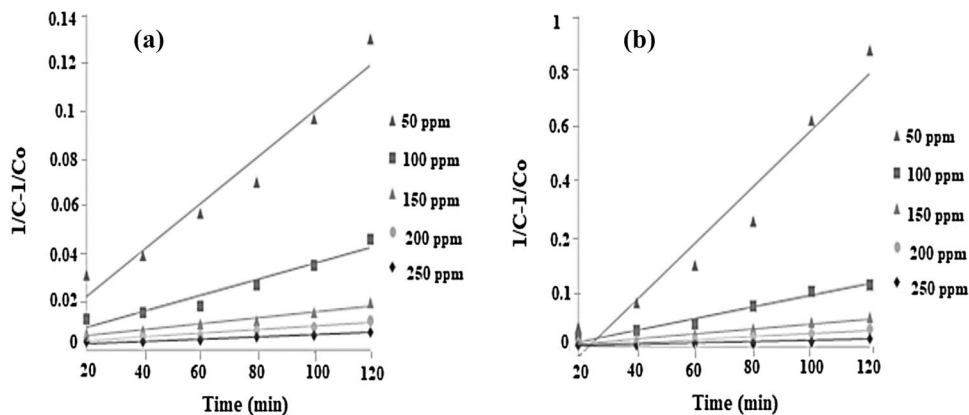
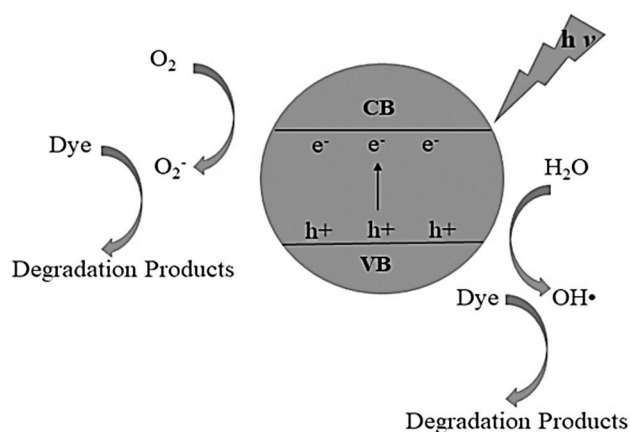


Fig. 11 Application of pseudo-second-order kinetics to photodegradation of dye on **a** undoped and **b** Nd-doped BaO at different initial concentrations of dye





Scheme 1 Proposed mechanism of the photodegradation of MG dye in the presence of UV light irradiation

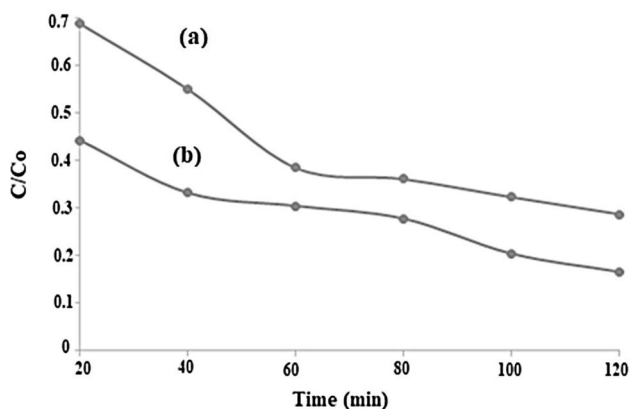


Fig. 12 Effect of dye initial concentration on degradation of dye on recovered undoped and recovered doped BaO

within 120 min irradiation time, while the recovered Nd-doped BaO degraded 83% dye within the same irradiation time. Similarly, the original undoped BaO degraded 86.6% within 120 min, while the recovered undoped BaO degraded about 71.2% within the same irradiation time. It was found that the activity of the recovered photocatalyst is lower than that of the original/fresh photocatalyst, which may be due to the photoactive hydroxide being deposited on the surface of the photocatalyst and blocking its active sites (Saeed et al. 2016).

Effect of photocatalyst dosage

The effect of a catalyst dose of 10–30 mg was tested at a pollutant concentration of 50 mg L⁻¹ (Fig. 13). It was observed that the dye degradation rate increased as the catalyst dose increased from 10 to 20 mg, and the degradation rate decreased beyond this. The increasing photodegradation rate

with increasing catalyst dose is attributed to the enhanced adsorption of photons due to the availability of more active sites. On the other hand, the photodegradation rate decreases with a further increase in catalyst dose leading to an increase in solution opacity ultimately decreasing the photon penetration (Wang et al 2014).

Effect of pH

The effect of pH in the range of 4–10 was tested at a pollutant concentration of 50 mg·L⁻¹ (Fig. 14). The undoped BaO degraded about 75% dye at pH 4. The Nd-doped BaO degraded about 92% dye at pH 4. The percent degradation for both the catalyst decreased as the pH increased. The photocatalyst surface is positively charged in acidic solution and negatively charged in alkaline solution. The degradation efficiency was found to be greater at low pH because the dye adsorbed more in an acidic medium due to electrostatic interaction between the anionic dye (MG) and the positively charged surface of the catalysts (Hou et al. 2018).

Effect of dye initial concentration

Under a constant irradiation time of 120 min and a catalyst amount of 0.02 g (Fig. 15), the photodegradation of MG dye at various dye concentrations (50, 100, 150, 200, and 250 ppm) was studied. For Nd-doped BaO and undoped BaO, maximum degradation efficiencies of 96.4% and 86.6% were achieved at low dye concentrations (50 ppm), respectively. Because an increase in the dye initial concentration increases the amount of dye adsorbed on the photocatalyst surface, as a result, the dye molecules will absorb a significant amount of UV-light rather than the photocatalyst consequently, decreasing light penetration to NPs surface. As the active sites were occupied by the dye molecules which lead to a decrease in the generation of hydroxyl radicals, and hence, the rate of photodegradation decreased (Wang and Fakhri 2020).

Effect of temperature

The effect of temperature changes on dye degradation was monitored at three different temperatures, i.e., keeping all other parameters unchanged, namely 30, 40 and 50 °C. Figure 16 shows that the degradation of the dye increases with increasing temperature. For Nd-doped BaO and undoped BaO, maximum degradation efficiencies of 95% and 83% were achieved at 50 °C, respectively. The photodegradation percent of dye molecules is gradually enhanced by increasing the temperature. An increase in temperature gives rise to the formation of bubbles in the solution, as a result, free radicals are produced. Moreover, the increase in temperature also aids in the degradation reaction to overcome

Fig. 13 Effect of catalyst dosage on photodegradation of dye on a undoped BaO and b Nd-doped BaO

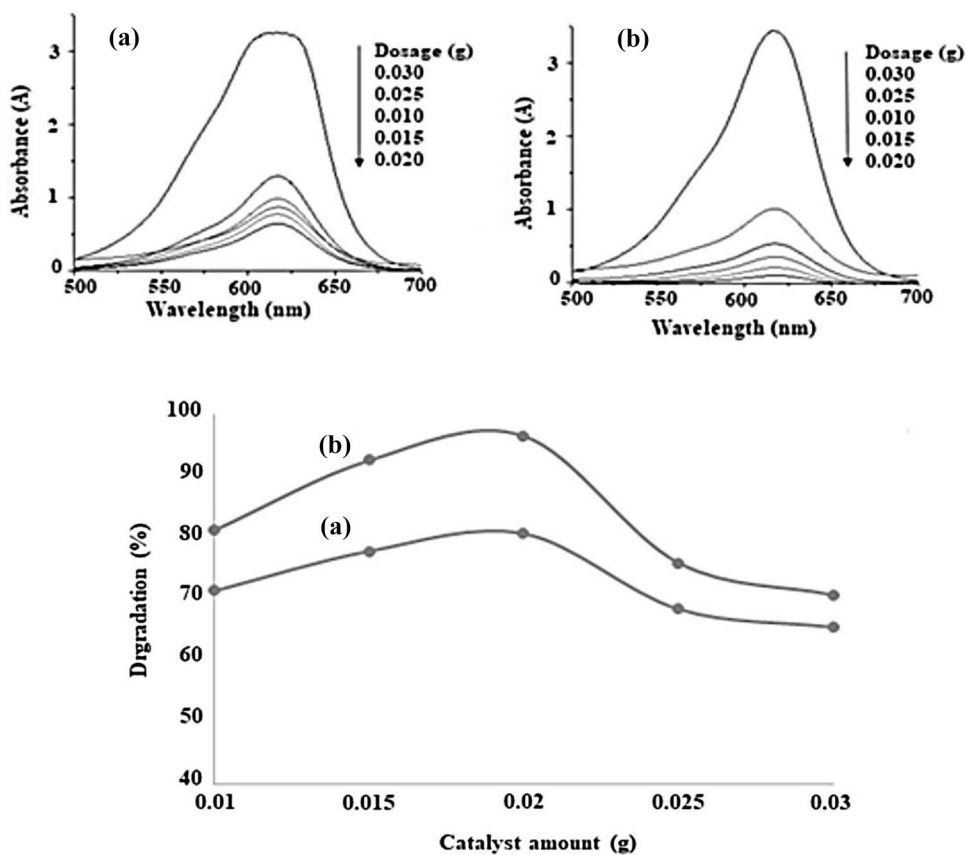


Fig. 14 Effect of pH on photodegradation of dye on a undoped BaO and b Nd-doped BaO

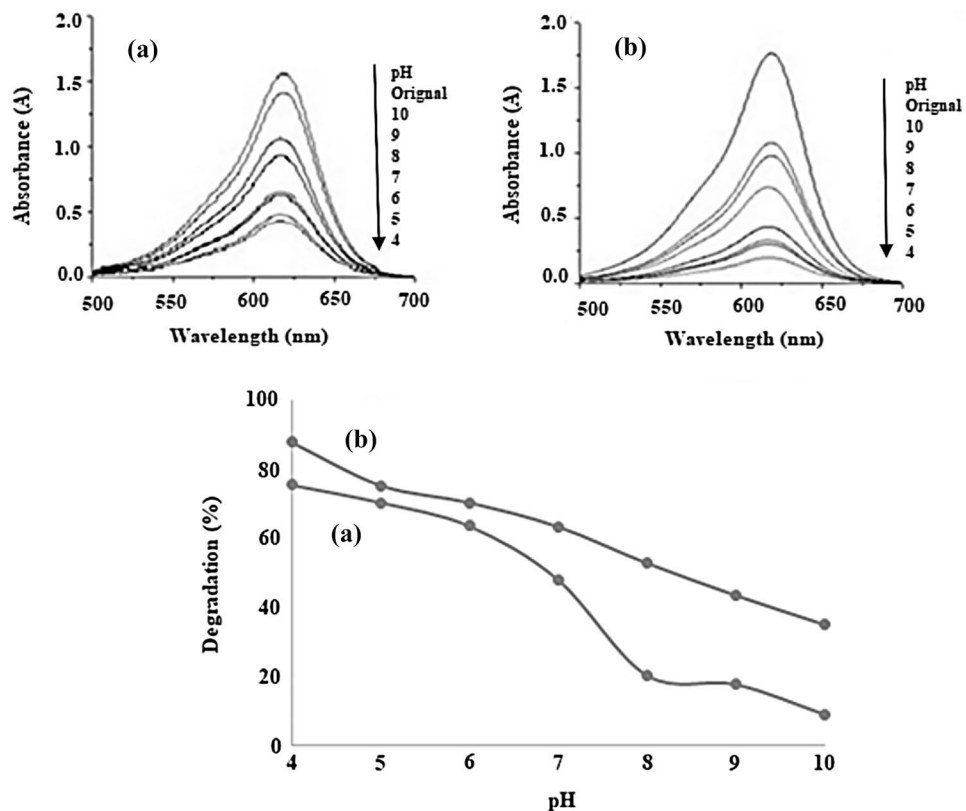


Fig. 15 Effect of dye concentration on degradation of dye on a undoped BaO and b Nd-doped BaO

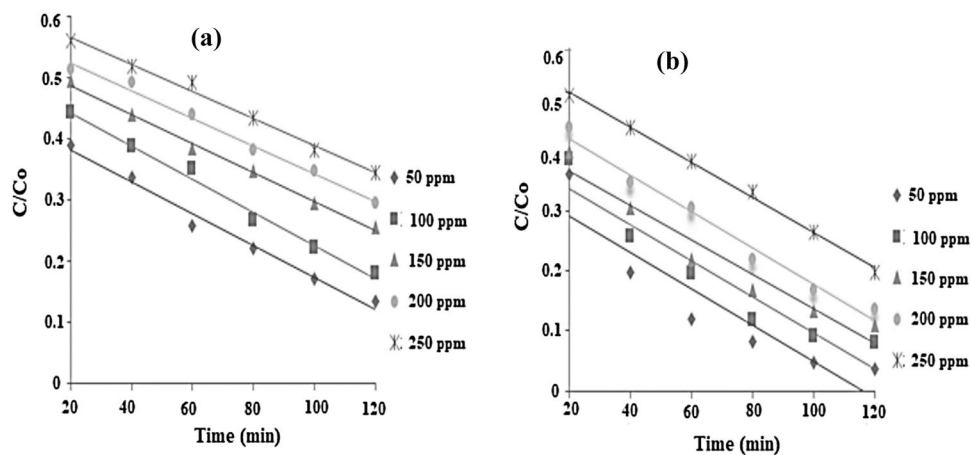
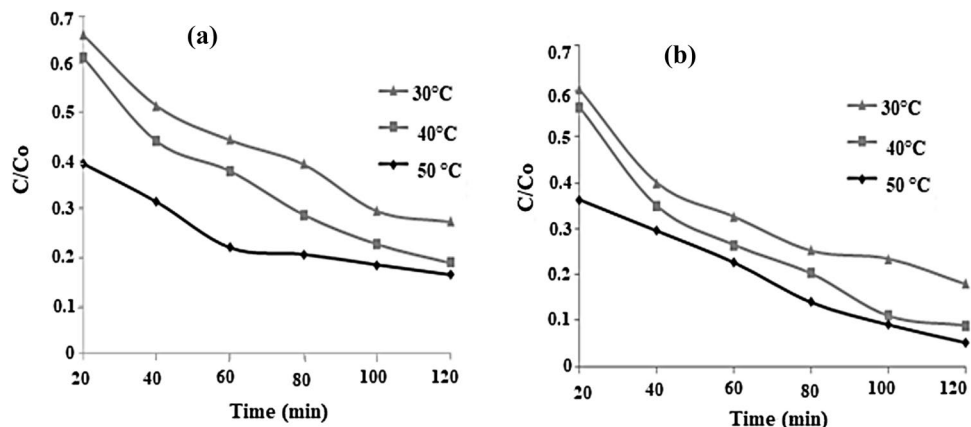


Fig. 16 Effect of temperature on the photocatalytic degradation of dye (reaction conditions: dye concentration = 100 mL, 50 mg/L, catalyst wt. 0.02 g on a undoped and Nd-doped b BaO



electron–hole recombination. By raising the temperature the oxidation rate of organic molecules is enhanced at the interface (Rafiq et al 2021).

Conclusion

It is concluded that the as-prepared catalysts were effective during the photodegradation of MG dye in an aqueous medium. The dye was efficiently degraded by the Nd-doped BaO than the undoped BaO. The dye was also degraded by the recycled photocatalysts but show less activity as compared to fresh catalyst due to the blocking of its active sites. The photodegradation rate increased as catalyst amount increased up to an optimal level. The photodegradation rate was found to be slightly higher at a low initial concentration of dye, low pH, and high temperature. It was also found that the first-order kinetics was better followed than the second-order kinetics model.

Acknowledgements The authors greatly acknowledge the technical support provided by the Department of Chemistry, Bacha Khan University, Charsadda, Khyber Pakhtunkhwa, Pakistan.

Funding The authors received no specific funding for this work.

Declarations

Conflict of interest The authors declare that there is no conflict of interest.

Open access This article is licensed under a Creative Commons Attribution 4.0 International License, which permits use, sharing, adaptation, distribution, and reproduction in any medium or format, as long as you give appropriate credit to the original author(s) and the source, provide a link to the Creative Commons license, and indicate if changes were made. The images or other third-party material in this article are included in the article's Creative Commons license unless indicated otherwise in a credit line to the material. If material is not included in the article's Creative Commons license and your intended use is not permitted by statutory regulation or exceeds the permitted use, you will need to obtain permission directly from the copyright holder. To view a copy of this license, visit <http://creativecommons.org/licenses/by/4.0/>.

Open Access This article is licensed under a Creative Commons Attribution 4.0 International License, which permits use, sharing, adaptation, distribution and reproduction in any medium or format, as long as you give appropriate credit to the original author(s) and the source, provide a link to the Creative Commons license, and indicate if changes were made. The images or other third party material in this article are included in the article's Creative Commons licence, unless indicated

otherwise in a credit line to the material. If material is not included in the article's Creative Commons licence and your intended use is not permitted by statutory regulation or exceeds the permitted use, you will need to obtain permission directly from the copyright holder. To view a copy of this licence, visit <http://creativecommons.org/licenses/by/4.0/>.

References

- Alnuaimi MM, Rauf MA, Ashraf SS (2007) Comparative decoloration study of neutral red by different oxidative processes. *Dyes Pigment* 72:367–371. <https://doi.org/10.1016/j.dyepig.2005.09.020>
- Avasarala BK, Tirukkavalluri SR, Bojja S (2016) Magnesium doped titania for photocatalytic degradation of dyes in visible light. *J Environ Anal Toxicol* 6:358. <https://doi.org/10.4172/2161-0525.1000358>
- Das M, Bhattacharyya KG (2014) Oxidation of Rhodamine B in an aqueous medium in ambient conditions with raw and acid-activated MnO₂, NiO, ZnO as catalysts. *J Mol Catal A Chem* 391:121–129. <https://doi.org/10.1016/J.MOLCATA.2014.04.019>
- Dobson RS, Burgess JE (2007) Biological treatment of precious metal refinery wastewater: a review. *Miner Eng* 20(6):519–532. <https://doi.org/10.1016/j.mineng.2006.10.011>
- Hou C, Hu B, Zhu J (2018) Photocatalytic degradation of methylene blue over TiO₂ pretreated with varying concentrations of NaOH. *Catalysts* 8:575. <https://doi.org/10.3390/catal8120575>
- Long T, Yin S, Takabatake K, Zhnag P, Sato T (2008) Synthesis and characterization of ZnO nanorods and nano disks from zinc chloride aqueous solution. *Nanoscal Res Lett* 4:247–253. <https://doi.org/10.1007/s11671-008-9233-2>
- Rafatullah M, Sulaiman O, Hashim R, Ahmad A (2010) Adsorption of methylene blue on low cost adsorbents. *J Hazard Mater* 177:70–80. <https://doi.org/10.1016/j.jhazmat.2009.12.047>
- Rafiq A, Ikram M, Ali S, Niaz F, Khan M, Khan Q, Maqbool M (2021) Photocatalytic degradation of dyes using semiconductor photocatalysts to clean industrial water pollution. *J Indus Eng Chem* 97:111–128. <https://doi.org/10.1016/j.jiec.2021.02.017>
- Ramasam V, Praba K, Murugadoss G (2012) Synthesis and study of optical properties of transition metals doped ZnS nanoparticles. *Spectrochim Acta, Part A* 96:963–971. <https://doi.org/10.1016/j.saa.2012.07.125>
- Saeed K, Ishaq M, Sultan S, Ahmad I (2015) Removal of methyl violet 2-B from aqueous solutions using untreated and magnetite-impregnated almond shell as adsorbents. *Desalin Water Treat* 57:13484–13493. <https://doi.org/10.1080/19443994.2015.1058191>
- Saeed K, Khan I, Sadiq M (2016) Synthesis of graphene-supported bimetallic nanoparticles for the sunlight photodegradation of basic green 5 dye in aqueous medium. *Separation Sci Technol* 51:1421–1426. <https://doi.org/10.1080/01496395.2016.1154872>
- Shah A, Shahzad S, Munir A, Nadagouda MN, Khan GS, Shams DF, Dionysiou DD, Rana UA (2016) Micelles as soil and water decontamination agents. *Chem Rev* 116:6042–6074. <https://doi.org/10.1021/acs.chemrev.6b00132>
- Sharma G, Kumar A, Sharma S, Naushad M, Dhiman P, Vo DVN, Stadler FJ (2020) Fe₃O₄/ZnO/Si₃N₄ nanocomposite based photocatalyst for the degradation of dyes from aqueous solution. *Mater Lett* 278:128359. <https://doi.org/10.1016/j.matlet.2020.128359>
- Shivaraju HP, Midhun G, Kumar KMA, Pallavi S, Pallavi N, Behzad S (2017) Degradation of selected industrial dyes using Mg-doped TiO₂ polyscales under natural sun light as an alternative driving energy. *App Water Sci* 7:3937–3948. <https://doi.org/10.1007/s13201-017-0546-0>
- Wang G, Fakhri A (2020) Preparation of CuS/polyvinyl alcohol-chitosan nanocomposites with photocatalysis activity and antibacterial behavior against G+/G- bacteria. *Int J Biologic Macromol* 155:36–41. <https://doi.org/10.1016/j.ijbiomac.2020.03.077>
- Wang X, Wu P, Huang Z, Zhu N, Wu J, Li P, Dang Z (2014) Solar photocatalytic degradation of methylene blue by mixed metal oxide catalysts derived from ZnAlTi layered double hydroxides. *Appl Clay Sci* 95:95–103. <https://doi.org/10.1016/j.clay.2014.03.016>
- Wang H, Xie CS, Zhang W, Cai S, Yang Z, Gui Y (2007) Comparison of dye degradation efficiency using ZnO powders with various size scales. *J Hazard Mater* 141:645–652. <https://doi.org/10.1016/j.jhazmat.2006.07.021>
- Wang Y, Zhang C, Bi S, Luo GS (2010) Preparation of ZnO nanoparticles using the direct precipitation method in a membrane dispersion micro-structured reactor. *Powder Technol* 202:130–136. <https://doi.org/10.1016/j.powtec.2010.04.027>
- Yaseen DA, Scholz M (2019) Textile dye wastewater characteristics and constituents of synthetic effluents: a critical review. *Int J Environ Sci Technol* 16:1193–1226. <https://doi.org/10.1007/s13762-018-2130-z>

Publisher's Note Springer Nature remains neutral with regard to jurisdictional claims in published maps and institutional affiliations.